

Facile synthesis of $\text{Li}_3\text{V}_2(\text{PO}_4)_3/\text{C}$ nano-flakes with high-rate performance as cathode material for Li-ion battery

Yanying Wang · Yan Tang · Benhe Zhong · Heng Liu · Yanjun Zhong · Xiaodong Guo

Received: 2 June 2013 / Revised: 6 August 2013 / Accepted: 31 August 2013 / Published online: 28 September 2013
© Springer-Verlag Berlin Heidelberg 2013

Abstract The flake-like $\text{Li}_3\text{V}_2(\text{PO}_4)_3/\text{C}$ has been successfully synthesized by rheological phase method using polyvinyl alcohol (PVA) as template; the $\text{Li}_3\text{V}_2(\text{PO}_4)_3/\text{C}$ without PVA assistance has been prepared for comparison. X-ray diffraction analysis shows that the two samples are well crystallized, and no impurity phases are detected. The scanning electron microscopy results reveal that there is a significant difference in morphologies between PVA-assisted sample and sample without PVA; the former shows a flake-like morphology, while the latter presents regular granular shape with some agglomeration. Transmission electron microscopy images reveal that $\text{Li}_3\text{V}_2(\text{PO}_4)_3$ particles are coated with a uniform surface carbon layer. The lattice fringes with a spacing of 0.428 nm can be clearly seen from the high-resolution transmission electron microscopy image. The PVA-assisted sample shows a discharge capacity of 120, 110, and 96 mAh g^{-1} at 1 C, 20 C, and 50 C, respectively; however, the sample without PVA exhibits a lower discharge capacity. Based on the analysis of electrochemical impedance spectroscopy, the lithium ion diffusion coefficients of $\text{Li}_3\text{V}_2(\text{PO}_4)_3/\text{C}$ and PVA-assisted $\text{Li}_3\text{V}_2(\text{PO}_4)_3/\text{C}$ are 4.19×10^{-9} and 4.99×10^{-8} $\text{cm}^2 \text{s}^{-1}$, respectively. In summary, it is demonstrated that using PVA as a template can obtain flake-like morphology and significantly improve the comprehensive electrochemical performances of $\text{Li}_3\text{V}_2(\text{PO}_4)_3/\text{C}$ cathode material.

Keywords $\text{Li}_3\text{V}_2(\text{PO}_4)_3/\text{C}$ · Polyvinyl alcohol · High-rate capability · Rheological phase method · Flake-like morphology

Introduction

Because the LiCoO_2 cathode material has the intrinsic drawbacks of being expensive and noxious, Li transition metal phosphate materials such as LiFePO_4 [1, 2], LiMnPO_4 [3], LiVPO_4F [4], and $\text{Li}_3\text{V}_2(\text{PO}_4)_3$ [5–7] have attracted much attention to acting as alternative cathode materials for lithium ion batteries. Among these materials, monoclinic structure $\text{Li}_3\text{V}_2(\text{PO}_4)_3$ has the advantages of having large theoretical capacity, good cryogenic property, and high operating voltage. However, $\text{Li}_3\text{V}_2(\text{PO}_4)_3$ suffers low electronic conductivity which limits the high-rate performance and hinders its wide application. A variety of efforts has been made to increase the electronic conductivity, such as carbon coating [8–10], metal doping [11], and particle size reduction [12]. It is confirmed that conductive carbon coating is the most efficient way [13]. Carbon coating on the surface of $\text{Li}_3\text{V}_2(\text{PO}_4)_3$ particles can not only enhance the electronic conductivity and suppress the particle agglomeration in the calcination procedure but also prevent the cathode material from directly contacting with the electrolyte solution, thus avoiding vanadium ions dissolving in the electrolyte [14, 15]. As far as we know, the influence of the surface carbon depends greatly on the type of carbon source and the synthesis method. Researchers usually choose the organic or polymer carbon sources for the reason of better dispersal ability, such as citric acid [16], oxalic acid [17], glucose [18], sucrose [19], stearic acid [20], ascorbic acid [21], polyvinyl alcohol [7], sugar [22], and so on. Rheological phase method [23] is an economical and effective soft chemical method that has no long time-consuming and any troublesome processes for preparing compounds or materials from

Y. Wang · Y. Tang · B. Zhong · Y. Zhong · X. Guo (✉)
College of Chemical Engineering, Sichuan University,
Chengdu 610065, People's Republic of China
e-mail: xiaodong2009@163.com

H. Liu
College of Materials Science and Engineering, Sichuan University,
Chengdu 610064, People's Republic of China

a solid–liquid rheological mixture. Besides, the key of this method is a liquid–solid rheological body including the solid particles and liquid molecules which are uniformly distributed. The surface area of the solid particles can be utilized efficiently due to the close and uniform contact between solid particles and fluid. However, no studies have yet been reported about the synthesis of the $\text{Li}_3\text{V}_2(\text{PO}_4)_3/\text{C}$ by using stearic acid as carbon source and polyvinyl alcohol (PVA) as template via rheological phase method.

In this work, a novel rheological phase method using PVA as a template has been introduced to synthesize $\text{Li}_3\text{V}_2(\text{PO}_4)_3/\text{C}$ composites and their electrochemical performances, and especially the high-rate charge–discharge property has been investigated.

Experimental

Preparation of the $\text{Li}_3\text{V}_2(\text{PO}_4)_3/\text{C}$ composites

$\text{Li}_3\text{V}_2(\text{PO}_4)_3/\text{C}$ composites were prepared via a novel rheological phase method by using LiH_2PO_4 , with V_2O_5 as the starting materials. Stearic acid was employed as carbon source, and the residual carbon decomposition from it during calcination process could be the reductant. The polyvinyl alcohol (PVA-1799) acted as a template reagent. The stearic acid and PVA also played an important role in dispersing the raw materials. Stoichiometric amounts of LiH_2PO_4 , V_2O_5 , and 4 wt% PVA were mixed together in proper ethanol by ball milling for 1 h in a high-speed vibrating ball miller (SFM-3, 1,200 rpm, MTI Corporation) in order to get a rheological body. After that, 24.5 wt% stearic acid which was dissolved in ethanol was added to the rheological body, and ball milling was continued for another 1 h to get the pasty precursor. The obtained pasty precursor was dried at 90 °C for 6 h in an air-dry oven to evaporate the ethanol. The dried precursor was reground and finally calcined at 700 °C for 4 h in a tube furnace under Ar atmosphere to obtain the $\text{Li}_3\text{V}_2(\text{PO}_4)_3/\text{C}$ composites. The $\text{Li}_3\text{V}_2(\text{PO}_4)_3/\text{C}$ without PVA assistance was prepared by the same process for comparison. The $\text{Li}_3\text{V}_2(\text{PO}_4)_3/\text{C}$ without PVA assistance was named sample A, and the PVA-assisted $\text{Li}_3\text{V}_2(\text{PO}_4)_3/\text{C}$ was named sample B.

Material characterizations

Thermogravimetry–derivative thermogravimetry–differential thermal analysis (TG-DTG-DTA) of the precursor was measured by TG-209F1 device at the temperature range from 30 to 1,000 °C at the heating rate of 10 °C min^{-1} under a N_2 flow of 20 ml min^{-1} . The residual carbon content of the material was tested by CS-902 analytical device. The structure and crystal-line parameters were analyzed by the X-ray diffraction (XRD, D/max-rB, Rigaku, by using $\text{Cu K}\alpha$ radiation with $\lambda =$

0.15046 nm). The morphology and size of $\text{Li}_3\text{V}_2(\text{PO}_4)_3/\text{C}$ particles were observed by scanning electron microscopy (SEM, SPA400 Seiko Instruments). The microscopic structure of the as-prepared sample was characterized by transmission electron microscope (TEM) and high-resolution transmission electron microscope (HRTEM) (JEM-2100, JEOL, Japan).

The battery preparation and electrochemical measurement

The working cathode is made up of 80 wt% active material (prepared $\text{Li}_3\text{V}_2(\text{PO}_4)_3/\text{C}$ powder), 13 wt% acetylene black that worked as the conducting agent, and 7 wt% polyvinylidene fluoride which served as the binder, and an appropriate amount of *N*-methyl-2-pyrrolidone was used as solvent. The obtained slurry was spread uniformly onto a thin and smooth aluminum foil and then dried at 100 °C for 10 h in a vacuum and cut into slices. The lithium metal foil was used as a counter electrode, Celgard 2400 as the separator, and 1 M LiPF_6 dissolved in a mixture of ethylene carbonate and dimethyl carbonate of 1:1 in volume as electrolyte. The cells were assembled in a glove box filled with high-purity argon. The calculated total mass loading for the electrodes are about 2.0 mg cm^{-2} . The charge–discharge measurements were recorded in the range of 3.0–4.5 V under different current densities at room temperature by employing a battery test system (NEWARE, China). Cyclic voltammetry (CV) was performed on a CHI660B electrochemical workstation at a scanning rate of 0.1 mV s^{-1} under the voltage range of 3.0–4.5 V. The electrochemical impedance spectroscopy (EIS) was measured by the as-prepared cells and recorded on the same electrochemical workstation over a frequency range from 100 kHz to 10 mHz with an AC amplitude of 5 mV.

Results and discussions

Material characterizations

Figure 1 shows the TG-DTG-DTA curves of sample B precursor from 30 to 1,000 °C. About 33.56 % weight loss of the precursor is observed from 30 to 700 °C. With the temperature increasing, low weight loss appears that it can be entirely neglected. According to the weight loss derivative curve, the weight loss curve can be sketchily divided into three parts. The first part below 160 °C is due to the release and evaporation of the adsorbed water. In previous reports, the pyrolysis of PVA occurred at 160 °C in nitrogen atmosphere and starts to abruptly decompose at 280 °C [24]. The second part between 160 and 400 °C is attributed to the volatilization and further thermal decomposition of stearic acid, which leads to the formation of reductive carbon, as well as the continuous elimination of hydrogen atom and oxygen atom, causing the pyrolysis of partial PVA and forming the conjugated double bond polymer. When the precursor is heated between 400 and 700 °C, a series

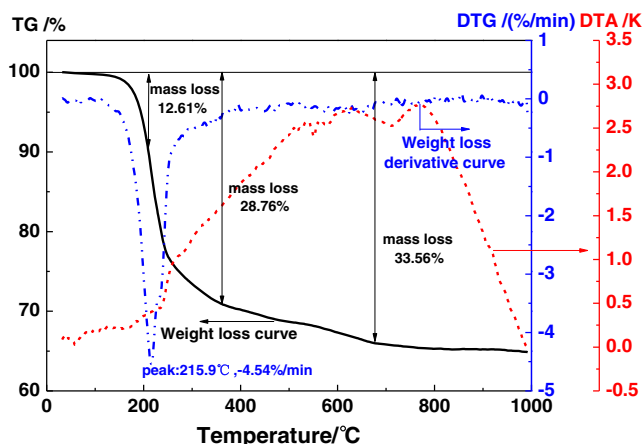


Fig. 1 TG-DTG-DTA curves of the sample B precursor recorded at the heating rate of 10 °C min⁻¹ under a N₂ flow of 20 ml min⁻¹

of complex reactions take place. This period contains the transformation of V⁵⁺ to V³⁺ by the reduction of carbon at the high temperature inside inert atmosphere, along with the release of carbon oxides as well. The well-crystallized Li₃V₂(PO₄)₃/C composites are obtained from the reaction of lithium source, vanadium source, phosphate source, and residual carbon. Therefore, based on the results of TG-DTG-DTA, 700 °C is chosen as the calcination temperature.

Figure 2 shows the XRD patterns for the as-prepared samples—sample A and sample B. They have the same phase, and no impurity phases are detected. The sharp diffraction peaks indicate that both samples are well crystallized, and they can be indexed well on the basis of monoclinic Li₃V₂(PO₄)₃ with a space group of P2₁/n [PDF no. 47-0107], which are consistent with the previous reports [25, 26]. The refinement structural parameters of sample A and sample B are summarized in Table 1, in which a slight difference exists. Element analysis of the final products reveals that the carbon content of sample A

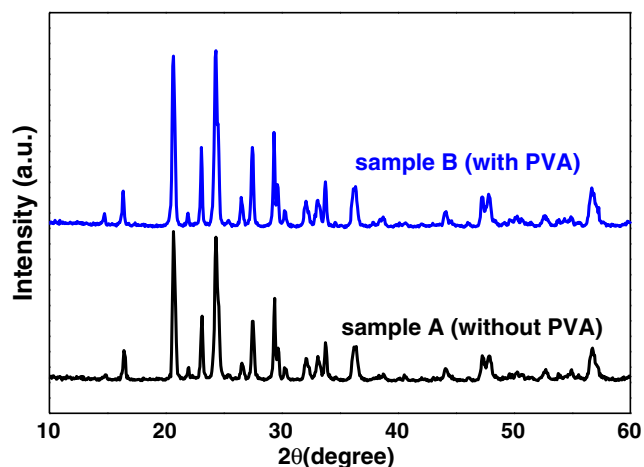


Fig. 2 X-ray diffraction patterns for the as-prepared sample A and sample B

and sample B are 3.05 and 3.18 %, respectively. However, there are no obvious diffraction peaks detected in relation to carbon, which indicates that the residual carbon from stearic acid or PVA is in amorphous state, or the carbon content coating on Li₃V₂(PO₄)₃ particles is too small to be detected.

Figure 3 shows the SEM images of sample A and sample B. The morphologies of sample A and sample B have a significant difference. It can be clearly observed that the particles of sample A present regular granular shape with some agglomeration. Moreover, the particle size distribution is narrow which ranges from 200 to 500 nm approximately. Sample B which is assisted with PVA has a flake-like morphology, and the lengths of the flakes are not uniform with the range of 1 to 2 μm; nevertheless, the shorter thicknesses of the flakes are 100 to 300 nm.

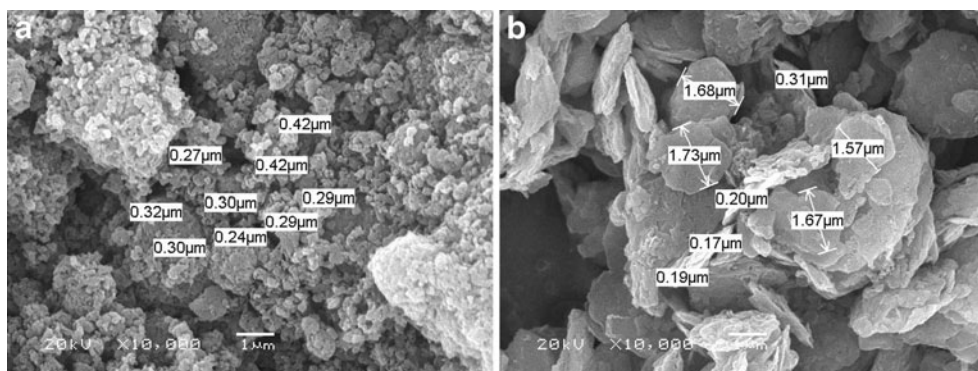
Figure 4 shows the TEM, high-resolution TEM (HRTEM), and the selected area electron diffraction (SAED) images of the as-prepared sample B. As shown in Fig. 4a, b, it can be clearly seen that the Li₃V₂(PO₄)₃ particles are coated with a uniform surface carbon layer. The surface carbon layer is favorable in enhancing conductivity and forming an efficient barrier to alleviate vanadium dissolution in the electrolyte solution. Figure 4c shows the HRTEM image taken from an individual Li₃V₂(PO₄)₃ particle; it can be seen that the lattice fringes appear clearly, indicating that the sample is well crystallized. The observed lattice fringes with a spacing of 0.428 nm corresponding to the (1 2 1) plane clearly confirm the monoclinic Li₃V₂(PO₄)₃ structure, which agrees well with the results of XRD. In order to show well the crystallinity of the as-prepared sample, the SAED image is presented in Fig. 4d, which indicates single crystal nature of Li₃V₂(PO₄)₃ nanoparticles in the Li₃V₂(PO₄)₃/C composites.

From the results of SEM and TEM images, sample A presents a regular granular shape with some agglomeration, while sample B which is assisted with PVA has a flake-like morphology. Many literatures have reported that PVA is a soft template which is widely used in controllable synthesis of nanoparticles [27, 28]; we can make a bold conjecture that PVA acting as a template plays an important role in changing the morphology of the Li₃V₂(PO₄)₃/C. PVA has a structure of planar zigzag; what is more, the hydroxyl of PVA can chelate vanadium (V₂O₅) and form a complex compound. When LiH₂PO₄, V₂O₅, and PVA are mixed together in proper ethanol, the starting materials (solid particles, namely LiH₂PO₄, V₂O₅,

Table 1 Lattice parameters of sample A and sample B

	Lattice parameters				
	<i>a</i> (Å)	<i>b</i> (Å)	<i>c</i> (Å)	β	<i>V</i> (Å ³)
Sample A (without PVA)	8.52	12.04	8.58	89.28	880.95
Sample B (with PVA)	8.53	12.07	8.59	89.49	884.55

Fig. 3 SEM images of the as-prepared samples: **a** sample A and **b** sample B



and PVA) can be dispersed efficiently by ethanol (fluid) in the rheological body. The surface area of the starting materials is completely naked to each other, which is a benefit to the reaction. And then, PVA reacts with V_2O_5 to form a complex compound, and LiH_2PO_4 attaches to the complex compound and self-assembles. After that, the stearic acid molecules are self-assembled homogeneously on the surface of the PVA

template. Finally, the flake-like $Li_3V_2(PO_4)_3/C$ sample is obtained by high-temperature calcination via the rheological phase method. PVA plays a role of the template that controls the synthesis of nanoparticles and directs the growth orientation of $Li_3V_2(PO_4)_3$ nano-flakes. The aforementioned product formation mechanism is simply presented in the schematic drawing, as shown in Fig. 5.

Fig. 4 TEM (a), TEM (b), HRTEM (c), and SAED (d) images of the as-prepared sample B

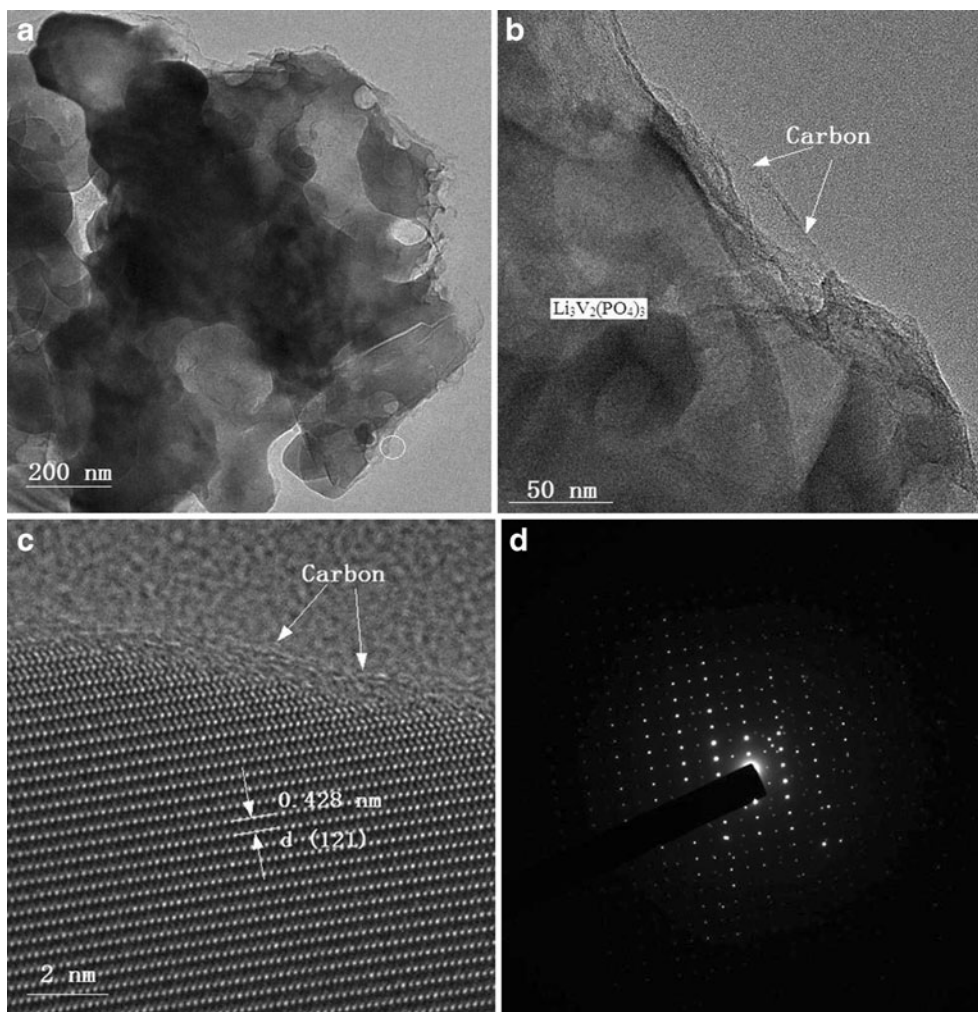
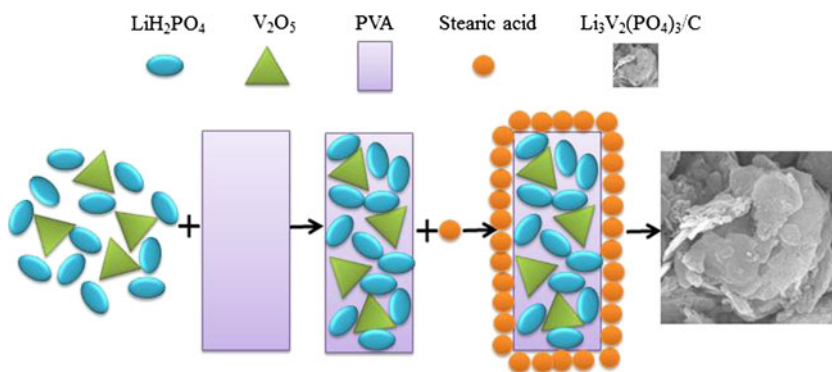


Fig. 5 Schematic drawing of the structure-templating mechanism by adding PVA as template

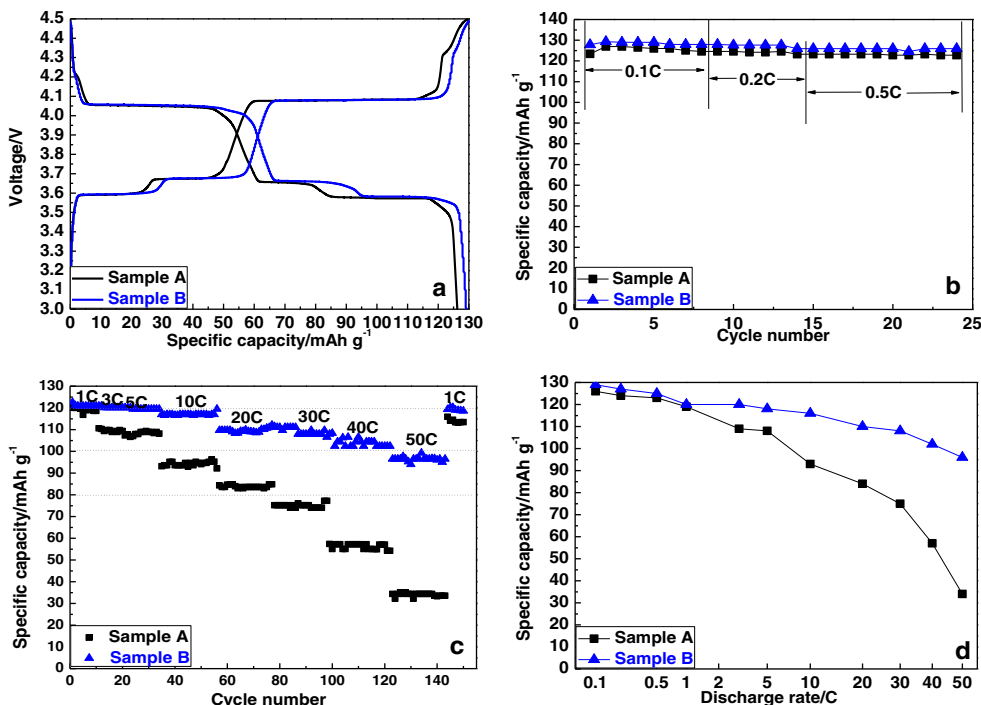


Electrochemical measurements

Figure 6 shows the initial charge/discharge curves at 0.1 C in the voltage range of 3.0~4.5 V and cycling performance for sample A and sample B at different discharge rates. As shown in Fig. 6a, the curves present three pairs of charge/discharge plateaus around 3.60/3.55, 3.68/3.65, and 4.10/4.05 V, respectively, which correspond to a series of phase transformations of $\text{Li}_3\text{V}_2(\text{PO}_4)_3$. The first two pairs of charge/discharge plateaus correspond to the reactions from $\text{Li}_3\text{V}_2(\text{PO}_4)_3$ to $\text{Li}_2\text{V}_2(\text{PO}_4)_3$ that an intermediate phase $\text{Li}_{2.5}\text{V}_2(\text{PO}_4)_3$ exists in the reaction. The intercalation/deintercalation of the second lithium ion takes place on the last pair of charge/discharge plateau with V^{3+} completely oxidized to V^{4+} . The potential differences of each pair of charge/discharge plateaus are very small that can even be neglected, indicating small electrode polarizations; in other words, the transportation of electrons and the diffusion of lithium ions in the electrodes goes through

easily. As shown in Fig. 6b, it can be seen fairly clear that the two samples possess large discharge capacity and little capacity fading at low discharge rate. For sample B, it delivers a discharge capacity of 129 mAh g^{-1} with the coulomb efficiency of 98.8 % at 0.1 C; however, for sample A, it is only 126 mAh g^{-1} with the coulomb efficiency of 97.3 % at the same rate. In Fig. 6c, the middle and high-rate capability of sample A and sample B are further compared in the voltage range of 3.0~4.5 V. The sample B shows a discharge capacity of 120, 116, 110, 108, and 102 mAh g^{-1} at 1 C, 10 C, 20 C, 30 C, and 40 C, respectively; however, sample A has a lower discharge capacity of 119, 93, 84, 75, and 57 mAh g^{-1} to the corresponding rate. At the rate of 50 C, the sample B delivers a discharge capacity of 96 mAh g^{-1} , which keeps 73.28 % of the theoretical capacity. Relatively, sample A delivers a lower discharge capacity of 34 mAh g^{-1} and about 25.95 % of the theoretical capacity than the PVA-assisted sample. What is more, sample A and sample B deliver a discharge capacity of

Fig. 6 **a** Initial charge/discharge curves for sample A and sample B at 0.1 C in the voltage range of 3.0~4.5 V. **b** Cycling performance at low discharge rate of sample A and sample B. **c** Cycling performance at middle and high discharge rate of sample A and sample B. **d** Rate performance for sample A and sample B at C-rate varying from 0.1 C to 50 C



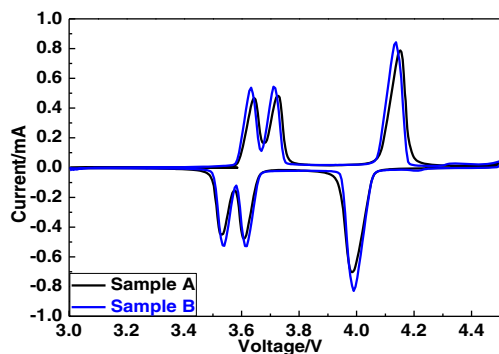


Fig. 7 The cyclic voltammetry curves of sample A and sample B under the voltage range of 3.0~4.5 V (vs Li^+/Li) at the scanning rate of 0.1 mV s^{-1}

113 and 119 mAh g^{-1} , respectively, when the rate returns to 1 C again after cycles at 50 C, demonstrating that high-rate cycling does not destroy the crystal structure, and the composites have the excellent reversibility. The further study on rate performance for the two samples at C-rate varying from 0.1 C to 50 C is displayed in Fig. 6d. Clearly, along with increasing discharge rate, sample B delivers a better discharge capacity and less attenuation ratio than sample A. The sample using PVA as a template presents a flake-like morphology and provides short diffusion lengths (about 100 to 300 nm) for electrons and lithium ions, which are believed to be helpful to the electrochemical performance.

Figure 7 shows the CV curves of sample A and sample B under the voltage range of 3.0~4.5 V at the scanning rate of 0.1 mV s^{-1} . It can be clearly seen that the CV curves of sample A and sample B are so similar. They both have three pairs of sharp redox peaks; corresponding to the first two lithium ions are inserted/extracted reversibility from the lattice of monoclinic $\text{Li}_3\text{V}_2(\text{PO}_4)_3$, which agree well with the charge–discharge curves in Fig. 6a. However, there are some differences between the two samples. Sample B has smaller potential distance between the cathodic peaks and the corresponding anodic peaks and higher current peak intensity than sample A, which demonstrate the better cycle reversibility and more wonderful kinetics properties.

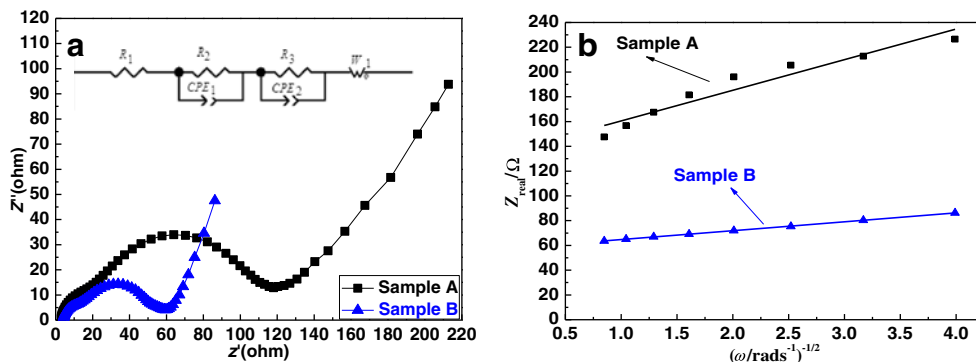
Table 2 Fitting impedance parameters according to the equivalent circuit and the diffusion coefficients of lithium ions, respectively

Number	$R_1 (\Omega)$	$R_2 (\Omega)$	$R_3 (\Omega)$	$D_{\text{Li}^+} (\text{cm}^2 \text{ s}^{-1})$
Sample A	2.868	12.73	95.47	4.19×10^{-9}
Sample B	4.004	6.63	42.45	4.99×10^{-8}

Electrochemical impedance spectroscopy (EIS) measurements are carried out to discuss the effect of adding PVA or not. What is more, EIS is considered to be a powerful technique to evaluate the diffusion coefficient of lithium ion [29], for the reason that the Warburg impedance in the low frequency is directly related to the lithium ion diffusion process in an electrode material [30]. Figure 8 shows the Nyquist plots of sample A and sample B, and the equivalent circuit used for imitating the experimental impedance data is shown in the inset. On the basis of the view of Barsoukov et al. [31], an intercept of the Z' -axis in the ultra-high-frequency region accords with the ohmic resistance (R_1), combining with the resistance of lithium ions and electrons getting through the electrolyte. The semicircle in the high-frequency region is the resistance that lithium ions get through the insulating layer of active material, R_2 is the resistance of solid electrolyte interface (SEI), and CPE_1 is the capacitance between SEI films. The semicircle in the middle-frequency region represents charge transfer resistance (R_3), the so-called electrochemical reaction resistance is in this zone as well, and CPE_2 is the electric double-layer capacity. The sloping line in the low-frequency region indicates the Warburg resistance (W_1), which is related to the diffusion of lithium ion in material particle [32].

In Fig. 8a, it can be seen clearly that R_3 of sample B is smaller than that in sample A, which indicates the contact resistance of $\text{Li}_3\text{V}_2(\text{PO}_4)_3$ particles is smaller; it may be the reason that sample B has higher rate capability. The fitting impedance parameters according to the equivalent circuit and the diffusion coefficient of lithium ions are presented in Table 2.

Fig. 8 **a** Nyquist plots of sample A and sample B. The equivalent circuit used for imitating the experimental impedance data is shown in the inset. **b** The relationship of impedance and angle frequency in the low-frequency region



The diffusion coefficients of lithium ions can be calculated by using the formula [29, 33] as follows:

$$D_{\text{Li}^+} = \frac{T^2 R^2}{2n^4 A^2 F^4 \sigma^2 C^2}$$

In this formula, T is the absolute temperature, R is the gas constant, n is the number of charge transfer, A is the surface area of cathode, F is the Faraday constant, C is the concentration of lithium ions, and σ is the Warburg constant which can be calculated by the relation of frequency and impedance, obeying the following formula:

$$Z_{\text{real}} = R_1 + R_2 + R_3 + \sigma\omega^{-1/2}$$

The ω is the angle frequency. According to this formula, the slope σ is obtained. The lithium ion diffusion coefficients of the two samples can be calculated by utilizing this σ in the first formula. The lithium ion diffusion coefficients of sample A and sample B are 4.19×10^{-9} and 4.99×10^{-8} $\text{cm}^2 \text{s}^{-1}$, respectively. It is well known that the larger lithium ion diffusion coefficient values, the easier they lead to electrochemical kinetics with Li^+ extraction. In other words, sample B has better lithium ion diffusion property, leading to faster Li^+ diffusion and better electrochemical performance.

Conclusions

The PVA-assisted $\text{Li}_3\text{V}_2(\text{PO}_4)_3/\text{C}$ was obtained by rheological phase method, and $\text{Li}_3\text{V}_2(\text{PO}_4)_3/\text{C}$ without PVA assistance was prepared for comparison. The SEM results show that the sample using PVA as a template displays a flake-like morphology with a thickness of 100–300 nm, which can provide short diffusion lengths and benefit for the transformation of electrons and lithium ions. A uniform surface carbon layer is coated on the surface of $\text{Li}_3\text{V}_2(\text{PO}_4)_3$ particles according to the TEM images. And it also can be clearly seen from the HRTEM image that the lattice fringes with a spacing of 0.428 nm corresponding to the (1 2 1) plane. It is demonstrated that the PVA-assisted sample achieves an outstanding rate capability, which delivers a discharge capacity of 120, 110, and 96 mAh g^{-1} in the voltage range of 3.0–4.5 V at 1 C, 20 C, and 50 C rates, respectively. However, the sample without PVA owning a regular granular shape exhibits a lower discharge capacity. The EIS results show that the PVA-assisted sample has smaller charge transfer resistance and bigger lithium ion diffusion coefficient compared with the sample without PVA. In summary, the sample using PVA as a template can effectively shorten diffusion lengths for electrons and lithium ions by controlling sizes and morphologies and make better the comprehensive electrochemical properties.

Acknowledgments This work was supported by the Sichuan University Funds for Young Scientists (no. 2011SCU11081) and the Research

Fund for the Doctoral Program of Higher Education, the Ministry of Education (no. 20120181120103).

References

- Liang GC, Wang L, Ou XQ, Zhao X, Xu SZ (2008) *J Power Sources* 184:538–542
- Tang H, Guo XD, Tang Y, Zhong BH, Li LY (2012) *Chin J Inorg Chem* 28:809–814
- Damen L, Giorgio FD, Monaco S, Veronesi F, Mastragostino M (2012) *J Power Sources* 218:250–253
- Zhong SK, Chen W, Li YH, Zou ZG, Liu CJ (2010) *Trans Nonferrous Metal Soc* 20:s275–s278
- Wang LJ, Liu HB, Tang ZY, Ma L, Zhang XH (2012) *J Power Sources* 204:197–199
- Yan J, Yuan W, Xie H, Tang ZY, Mao WF, Ma L (2012) *Mater Lett* 71:1–3
- Wei JW, Zhang XF, Liu J, Yang GL, Ge YC, Yu ZJ, Wang RS, Pan XM (2010) *Electrochim Acta* 55:6879–6884
- Li YJ, Hong L, Sun JQ, Wu F, Chen S (2012) *Electrochim Acta* 85: 110–115
- Jian ZL, Zhao L, Wang R, Hu YS, Li H, Chen W, Chen LQ (2012) *RSC Adv* 2:1751–1754
- Ding ZJ, Zhao L, Suo LM, Jiao Y, Meng S, Hu YS, Wang ZX, Chen LQ (2011) *Phys Chem Chem Phys* 13:15127–15133
- Yao JH, Wei SS, Zhang PJ, Shen CQ, Aguey-Zinsou KF, Wang LB (2012) *J Alloys Compd* 532:49–54
- Hao WJ, Zhan HH, Yu J (2012) *Mater Lett* 83:121–123
- Rui XH, Li C, Chen CH (2009) *Electrochim Acta* 54:3374–3380
- Fu P, Zhao YM, An XN, Dong YZ, Hou XM (2007) *Electrochim Acta* 52:5281–5285
- Zhang LL, Liang G, Peng G, Zou F, Huang YH, Croft MC, Ignatov A (2012) *J Phys Chem* 116:12401–12408
- Chen QQ, Wang JM, Tang Z, He WC, Shao HB, Zhang JQ (2007) *Electrochim Acta* 52:5251–5257
- Pan AQ, Liu J, Zhang JG, Xu W, Cao GZ, Nie ZM, Arey BW, Liang SQ (2010) *Electrochem Commun* 12:1674–1677
- Wang L, Zhang LC, Lieberwirth I, Xu HW, Chen CH (2010) *Electrochem Commun* 12:52–55
- Jiang T, Du F, Zhang KJ, Wei YJ, Li Z, Wang CZ, Chen G (2010) *Solid State Sci* 12:1672–1676
- Qiao YQ, Wang XL, Xiang JY, Zhang D, Liu WL, Tu JP (2011) *Electrochim Acta* 56:2269–2275
- Huang JS, Yang L, Liu KY (2011) *Mater Chem Phys* 128:470–474
- Jian ZL, Zhao L, Pan HL, Hu YS, Li H, Chen W, Chen LQ (2012) *Electrochem Commun* 14:86–89
- Chang CX, Xiang JF, Shi XX, Han XY, Yuan LJ, Sun JT (2008) *Electrochim Acta* 53:2232–2237
- Nakajima C, Saito T, Yamaya T, Shimoda M (1998) *Fuel* 77:321–326
- Wang LJ, Tang ZY, Ma L, Zhang XH (2011) *Electrochem Commun* 13:1233–1235
- Pan AQ, Choi D, Zhang JG, Liang SQ, Cao GZ, Nie ZM, Arey BW, Liu J (2011) *J Power Sources* 196:3646–3649
- Xie RM, Xiao DB, Yao JN (2002) *Acta Phys Chim Sin* 18:34–38
- Jiu JT, Li LP, Ge Y, Zhang SR, Tu F, Hua ZR, Nie L (2001) *Chin J Inorg Chem* 17:361–365
- Du XY, He W, Zhang XD, Yue YZ, Liu H, Zhang XG, Min DD, Ge XX, Du Y (2012) *J Mater Chem* 22:5960–5969
- Zeng RH, Li WS, Lu DS, Huang QM (2007) *J Power Sources* 174: 592–597
- Zhuang QC, Xu SD, Qiu XY, Cui YL, Fang L, Sun SG (2010) *Process Chem* 22:1044–1057
- Barsoukov E, Kim JH, Yoon CO, Lee H (1998) *J Electrochem Soc* 145:2711–2717
- Cui Y, Zhao XL, Guo RS (2010) *Electrochim Acta* 55:922–926